Food Chemistry: X 24 (2024) 101927

Contents lists available at ScienceDirect

Food Chemistry: X

journal homepage: www.sciencedirect.com/journal/food-chemistry-x

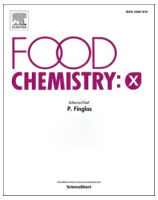

Recovery of protein-rich biomass from surimi rinsing wastewater by using a sustainable cold plasma treatment

Xin Wang [a,1], Mengzhe Li [a,1], Tong Shi [a,*], Abdul Razak Monto [a], Li Yuan [a], Wengan Jin [b], Ruichang Gao [a,b,c,*]

[a] School of Food and Biological Engineering, Jiangsu University, Zhenjiang 212013, China
[b] Bio-resources Key Laboratory of Shaanxi Province, School of Biological Science and Engineering, Shaanxi University of Technology, Hanzhong 723001, China
[c] Quanzhou Marine Biotechnology Industry Research Institute, Quanzhou 362700, China

ARTICLE INFO

Keywords:
Protein recovery
Cold atmospheric plasma jet
Molecular structure
Surimi rinsing wastewater
Proteomics

ABSTRACT

Surimi rinsing wastewater is typically discarded, causing waste of protein resources and environmental pollution. This study investigated the technology of a cold atmospheric plasma jet (CAPJ) for the recovery of protein-rich biomass (PRB), including myofibrillar proteins (MPs) and sarcoplasmic proteins (SPs), from surimi rinsing wastewater. The protein recovery yield was up to 59.84 %. CAPJ induced an increase in carbonyl and decreased sulfhydryl in protein content. Furthermore, the secondary structure of the protein was unfolded, particularly the transition from α-helix to β-sheet. The formation of disulfide bonds and increased hydrophobic interactions promoted protein aggregation (the particle size from 185.76 nm to 1869.07 nm, $P < 0.05$) and reduced solubility. The proteomic results indicated that CAPJ increased the expression level of antioxidant enzymes. Overall, the CAPJ technology could recover proteins from surimi rinsing wastewater for industrial application, which will promote the sustainable development of the surimi industry.

1. Introduction

Surimi products are favored among customers, particularly in Eastern Asia (Li et al., 2022). The production of surimi products mainly includes rinsing, chopping, and heating surimi (Zhang et al., 2021). Among them, rinsing is a necessary and crucial step, eliminating unfavorable factors such as sarcoplasmic proteins (SPs), lipids, enzymes and blood in fish meat, in order to obtain good gel texture (Gehring et al., 2011; Tadpitchayangkoon, Park, Mayer, & Yongsawatdigul, 2010). The rinsing water consumption of 1 ton of surimi is 10–15 tons, and the protein content in the rinsing wastewater is about 10–30 g/L (Zhang et al., 2022). As a result, surimi rinsing causes a waste of protein resources and negatively affects the environment. Based on the significant value of proteins on the market and the sustainability of the surimi industry, these are the motivations for finding cost-effective recycling technologies that can return these compounds to the food chain. Currently, the main methods for recovering protein from wastewater are membrane separation, flocculation, and isoelectric point precipitation, but there are difficulties with commercial application and safety issues with metal ions or residues of synthetic/non-food grade polymers, which are unsustainable treatment of valuable resource (Tadpitchayangkoon, Park, & Yongsawatdigul, 2010; Zhao et al., 2019). Finding sustainable and cost-effective recycling technologies could provide an entirely new type of biomass during the rinsing process of surimi, which could then be used as a protein component in food production.

Cold plasma is a recently developed non-thermal treatment technology that has gained attention in the fields of biology, medicine, and food research due to its residue-free, environmentally friendly, sustainable and cost-effective characteristics (Ekezie et al., 2019). Cold plasma is an ionised gas containing many reactive substances such as electrons, excited state atoms, free radicals, etc. (Cheng et al., 2023). The active substances in cold plasma could change the function of proteins by modifying protein microstructure (Liu, Tang, et al., 2024; Lv et al., 2024; Ke et al., 2023; Li et al., 2022). Our earlier studies showed that cold plasma treatment could promote the aggregative process of fish myofibrillar proteins (MPs) through alterations in the pH and zeta potential induced by reactive substances (Li et al., 2022; Li et al., 2024). In light of these considerations, we speculated that cold plasma, a novel

* Corresponding author at: School of Food and Biological Engineering, Jiangsu University, No.301, Xuefu Road, Zhenjiang, Jiangsu Province 212013, China.
E-mail addresses: 1000005720@ujs.edu.cn (T. Shi), xiyuan2008@ujs.edu.cn (R. Gao).
[1] These authors contributed equally to this work.

https://doi.org/10.1016/j.fochx.2024.101927
Received 3 September 2024; Received in revised form 15 October 2024; Accepted 23 October 2024
Available online 24 October 2024

and environmentally benign technology, could potentially be applied to recover PRB from surimi rinsing wastewater by facilitating protein aggregation.

The aim of this study was to recover PRB from surimi rinsing wastewater by CAPJ technology. We further elucidated the potential mechanism behind cold plasma on recovering PRB by exploring the alteration of physicochemical properties and composition of proteins in PRB. This research may offer a theoretical foundation and a new method for the recovery of proteins from wastewater produced in the food industry by cold plasma.

2. Materials and methods

2.1. Materials and chemicals

Live bighead carp (*Hypophthalmichthys molitrix*) (average weight 1.4–2.2 kg) was obtained from Jimailong supermarket (Zhenjiang, China), then knocked unconscious by a wooden stick. To prevent denaturation of fish proteins above 4 °C and to ensure the freshness of the fish, the fish were transported to the laboratory in boxes filled with ice. Then, the fish were stripped of the scales, heads, and internal organs, and cleaned. Afterwards, the fish skin and bones were removed by a flesh separator (HZ150, Hongxu Food Machinery Co., Ltd., Zhucheng, China), and the fish minces were stirred evenly and gathered. The experimental process conformed to the Guidance on Treating Experimental Animals developed by China's Ministry of Science & Technology in 2006 and Regulations issued by the China State Council in 1988. The fish minces were kept at 4 °C for the next experiment for not more than 24 h. All other chemicals and reagents were of analytical grade and sourced from Sinopharm Chemical Reagent Co., Ltd., Shanghai, China.

2.2. Recovery proteins from surimi rinsing wastewater

According to Zhang et al. (2022), the fish minces were rinsed with 5 volumes (*w/v*) of 0.02 M cold Tris-HCl buffer comprising 0.1 M NaCl (pH 7.0) for 5 min at 4 °C. All rinsed bighead carp minces were centrifuged (10,000 ×*g*, 15 min, 4 °C), and the supernatant was collected as the surimi rinsing wastewater. The surimi rinsing wastewater was treated with a cold atmospheric plasma jet (CAPJ) using the high-performance digitized plasma generator (PG-1000 ZD, Suman Plasma Technology Co., Ltd., Nanjing, China). Once the requisite parameters for the treatment had been established (power 15 W, voltage 12 V, and current 1.2 A), the plasma spray gun was positioned approximately 10 cm above the surimi rinsing wastewater (300 mL). Before centrifugation at 10,000 ×*g* for 15 min at 4 °C, the surimi rinsing wastewater was exposed to the CAPJ for 0 min, 10 min, 20 min, 30 min and 40 min to recover the precipitate as protein-rich biomass (PRB), named PRB_0, PRB_{10}, PRB_{20}, PRB_{30} and PRB_{40}, respectively. The temperature was kept below 25 °C during the entire treatment.

2.3. pH and H_2O_2 determination

H_2O_2 is considered the primary active substance generated in solution during cold plasma treatment (Li et al., 2022). In addition, the solution's pH value may result from significant change induced by CAPJ. Therefore, the surimi rinsing wastewater's pH value and H_2O_2 changes were measured per 5 min during CAPJ treatment. The pH value of the surimi rinsing wastewater was measured using a pH meter (PHSJ-3F, INESA Scientific Instrument Co., Ltd., Shanghai, China).

According to the method of Cheng et al. (2021), an H_2O_2 kit (Beyotime Biotechnology Ltd., Shanghai, China) was utilized to quantify the H_2O_2 content in the surimi rinsing wastewater. Following a 30 min incubation at room temperature in the absence of light, the absorbance of the sample at 540 nm was measured using a microplate reader (Multiskan FC, Thermo Fisher Instruments Ltd., Shanghai, China).

2.4. Determination of protein recovery yield

The aggregation behavior of SPs was affected by pH, showing that protein could be recovered by the pH-shift process (Tadpitchayangkoon, Park, Mayer, & Yongsawatdigul, 2010).Two methods were selected for the treatment of the surimi rinsing wastewater: i) CAPJ treatment group: treated with CAPJ (10 min, 20 min, 30 min, and 40 min); ii) pH treatment group: adjustment of pH value with HCl (according to the pH values in 2.3 section of different times, adjusted the pH values of the rinsing solution be the same as the former). According to the method by Tadpitchayangkoon, Park, and Yongsawatdigul (2010) with some modifications, the suspensions were centrifuged for 15 min (10,000 ×g, 4 °C), and the supernatants were collected. The protein concentration was quantified by the biuret method, employing bovine serum albumin as a standard for calibration. The protein recovery yield was calculated as follows:

$$\textit{Recovery yield}\ (\%) = \left(1 - \frac{C_1}{C_2}\right) \times 100$$

C_1 is the protein concentration of the supernatant obtained after centrifugation, and C_2 is the protein concentration of the original rinsing solution.

2.5. Proximate analysis of PRB

The protein, lipid, and ash contents of PRB were determined according to the Chinese National Standard (GB 5009.5–2016, GB 5009.6–2016 and GB 5009.4–2016).

2.6. Determination in particle size of protein aggregates

The moderate H_2O_2 can facilitate the aggregation of proteins and enlarge the particle size (Li et al., 2024). Two methods were available for the treatment of surimi rinsing wastewater: i) CAPJ treatment group: treated with CAPJ (0 min, 10 min, 20 min, 30 min, and 40 min); ii) H_2O_2 treatment group: treated with different concentrations of H_2O_2 (according to the H_2O_2 contents in 2.3 section of different times, added with different concentrations of H_2O_2 of the rinsing solution be the same as the former). The particle sizes of the protein aggregates were determined according to the method of Luo et al. (2022). The protein concentration of the samples was adjusted to 0.1 mg/mL by the addition of 0.02 mol/L cold Tris-HCl with 0.1 mol/L NaCl (pH 7.0), then the particle size was measured using a Zetasizerlab (Malvern Instruments Ltd., Worcestershire, UK). Malvern Standard Operation Procedure software was applied to evaluate the particle sizes of the protein aggregates.

2.7. Thiobarbituric acid reactive substances (TBARS) value

The TBARS was determined according to Li et al. (2023) with minor modifications. Briefly, 10 mL of PRB solution (protein, 10 mg/mL) was mixed with 20 mL of 7.5 % (*w/v*) TCA solution, then centrifuged for 15 min (10,000 ×g, 4 °C). The collected supernatant (5 mL) was combined with 5 mL of 20 mM TBA solution. After being heated in a boiling water bath (99 °C) for 30 min, the mixture was cooled for 30 min at room temperature. The absorbance of the samples was measured at 532 nm using a UV/visible spectrophotometer (UV 1910, Shanghai Lingguang Technology Co., Ltd., Shanghai, China) and the values were recorded as mg malondialdehyde (MDA)/kg protein.

2.8. Determination of carbonyl content and total sulfhydryl group (-SH)

According to the method of Sharifian et al. (2019), the carbonyl content was determined. Two equal volumes (1.6 mL) of PRB solution (protein, 5 mg/mL) were prepared, one mixed with 3.2 mL of HCl (3 M) and the other mixed with 3.2 mL of 2,4-dinitrophenyl hydrazine (DNPH,

0.15 %, m/v, dissolved in 3 M HCl). After 30 min of dark incubation, each solution was added TCA (1.6 mL, 40 %, *w/v*) to terminate the reaction. Centrifuged at 10,000 ×*g* for 5 min, collected and rinsed the precipitates three times with 2 mL of an ethanol/ethyl acetate solution (1:1, *v*/v). Then, the precipitates were dissolved in 6 mL of 6 M guanidine hydrochloride, and the composites were incubated for 15 min at 37 °C. The absorbances of the mixtures were measured at 370 nm and 280 nm. The equation for calculating the carbonyl content was as follows:

$$Carbonyl\ content\ (nmol/mg\ protein) = \frac{A_{s370} - A_{c370}}{22000 \times [A_{s280} - (A_{s370} - A_{c370})] \times 0.43} \times 10^6$$

where A_{c370} and A_{s370} represent the absorbance of the blank and sample at 370 nm, respectively, and A_{s280} represents the absorbance of the sample at 280 nm.

The -SH content of protein was determined by Luo et al. (2022). Briefly, 4.5 mL of 8 M urea, 1 % SDS (*w/v*) and 3 mM EDTA (pH 8.0) were added to the PRB solution (protein, 10 mg/mL) and then mixed evenly. Subsequently, 4.0 mL of the mixture was reacted with 0.5 mL of 10 mM DTNB (pH 8.0) for 25 min at 40 °C. The absorbances of the mixtures were measured at 412 nm. The content of SH was calculated as follows:

$$-SH\ (mol/10^5 protein) = \frac{A_{412} \times 11.25}{13600 \times protein\ concentration}$$

where A_{412} represents the absorbance of the sample.

2.9. Determination of dityrosine and Schiff base content

According to Li et al. (2023), the Schiff base and dityrosine contents were measured using a fluorescence spectrophotometer (F98, Shanghai Lengguang Technology Co., Ltd., Shanghai, China). The protein concentration of the sample was adjusted to 0.1 mg/mL. The fluorescence intensity was quantified at an excitation/emission wavelength of 325/420 nm. The relative content of dityrosine was determined by calculating the ratio of estimated fluorescence intensity to protein concentration. For each sample, the emission spectra were scanned from 400 to 500 nm with an excitation wavelength of 350 nm. The fluorescence intensity at 460 nm was measured to determine the Schiff base level.

2.10. Structural characterization

2.10.1. Raman spectroscopy analysis

The protein secondary structure analysis was determined using the Raman microscope (DXR, Thermo Fisher Scientiffc Inc., USA), as reported by Sharifian et al. (2019). Briefly, the typical spectra of samples were recorded at 2 cm^{-1} resolution with 500–1900 cm^{-1}. The pertinent measuring parameters were scanned 3 times, at an exposure time of 60 s, sampling speed of 120 cm^{-1}/min, and the data was collected every 1 cm^{-1}. PeakFit 4.0 was used to calculate the protein secondary structure (α-helix, β-sheet, β-turn and random coil) content.

2.10.2. Fluorescence measurement

The PRB solutions (protein, 0.5 mg/mL) were scanned in the 300–450 nm range, with the excitation wavelength set at 280 nm (Cheng et al., 2023). The width of the excitation/emission slit was established at 5 nm.

2.11. Surface hydrophobicity

According to Li et al. (2024), bromophenol blue (BPB) was used to measure surface hydrophobicity. Firstly, 1 mL of PRB solutions (protein, 5 mg/mL) were reacted with 200 μL of BPB (1 mg/mL) for 2 h at 25 °C. After centrifugation (15 min at 8000 ×*g*, 4 °C), the supernatant was diluted with buffer solution (0.02 mol/L cold Tris-HCl with 0.1 mol/L NaCl at pH 7.0). The absorbance was measured at 595 nm and calculated as follows:

$$BPB\ bound\ (\mu g) = \frac{200 \times (A_{s595} - A_{c595})}{A_{c595}}$$

where A_{c595} and A_{s595} represent the absorbances of the blank and sample, respectively.

2.12. Determination of isoelectric point (pI)

The pI of protein was determined as described by Yu et al. (2023) with some modifications. After mixing PRB (1.5 g) with distilled water (25 mL), 25 mL of 1 M NaOH was added to the mixture to dissolve the proteins completely. Then, 50 mL of acetic acid (HAC, 1 M) was dissolved into a mixture under stirring. The protein solution was poured into a 250 mL volumetric flask, supplemented to the mark with distilled water, to prepare the protein glue. The protein glue (15 mL) was transferred to the injection bottle, adjusted to the desired pH with HAC, and finally, the volume was adjusted to 35 mL with distilled water. According to Table 1, the protein glue with different pH values was prepared. The protein precipitation was observed, and the turbidity and Zeta potential of the protein suspension was measured by a UV–vis-NIR spectrophotometer (UV-1800, Shimadzu Co., Kyoto, Japan) and a laser particle size analyzer (Malvern Instruments, UK), respectively.

2.13. SDS-PAGE analysis and protein identification

The analysis of SDS-PAGE was referred to the method of Ekezie et al. (2019), with slight modifications. Briefly, the PRB suspension (protein, 5 mg/mL) was mixed with loading buffer (2 % SDS, 0.006 % BPB and 20 % glycerine) in a 4:1 ratio. The mixtures were heated in a metal bath at 95 °C for 10 min before cooling to room temperature. Then, 10 μL of the sample was introduced into the gel, containing 12 % running gel and 4 % stacking gel.

According to the method of Liu, Tan, et al. (2024), the protein bands were cut from the gels for protein identification. Firstly, the gel pieces were decolorized using 500 μL of destaining solution (50 mM ammonium bicarbonate (NH_4HCO_3), 50 % acetonitrile (ACN)), followed by the addition of 13 ng/μL trypsin solution (dissolved with 50 mM NH_4HCO_3) to digest gel pieces. After an overnight 37 °C incubation, a final concentration of 1 % trifluoroacetic acid (TFA) was added to the sample to terminate the digestion process. Finally, 0.1 % TFA with 60 % acetonitrile (ACN) and 0.1 % TFA with 90 % ACN were used to extract peptides from gel pieces. The peptide was dried in a speed vacuum concentrator after desalination by Pierce C18 Spin Tips. The peptides were re-dissolved in 0.1 % (*w/v*) formic acid and analyzed using an Orbitrap Q-Exactive Plus coupled to an EASY-nanoLC 1200 system (Thermo Fisher Scientific, MA, USA). Carbamidomethyl on Cysteine was specified as the fixed modification. Oxidation on methionine, Deamidation on asparagine and glutamine, Acetylation on Protein N-term

Table 1
Preparation of different pH solutions.

Test tube number	1	2	3	4	5	6	7	8	9	10	11	12	13	14	15
pH	6.4	6.1	5.8	5.5	5.2	4.9	4.6	4.5	4.4	4.3	4.2	4.1	4.0	3.7	3.4

were specified as the variable modifications. The raw data were operated and analyzed by the PEAKS Studio software and against the database of UniProt database (*Hypophthalmichthys nobilis*, version 2023, 431 entries). The peptides with 1 % FDR and the proteins with 1 % FDR and containing at least 1 unique peptide were filtered.

2.14. DIA proteomics analysis

2.14.1. Protein digestion

Briefly, the protein samples were mixed with 50 μL of Lyse buffer under agitating (1000 r/min) at 95 °C for 10 min. After adding trypsin digestion buffer at room temperature, the samples were stirred at 37 °C for 2 h at 500 r/min. The digestion process was terminated by a Stop Buffer with a wash buffer to clean and desalt the sample in the cartridge. The peptides in the iST cartridge were cleaned and desalted for lyophilizing by SpeedVac.

2.14.2. Peptide separation and MS analysis

The peptides were redissolved with 0.1 % (w/v) formic acid and then subjected to Orbitrap Eclipse coupled to an EASY-nanoLC 1200 system (Thermo Fisher Scientific, MA, USA) analysis.

2.14.3. Protein identification and bioinformatics analysis

The DIA data analysis was conducted via Spectronaut 18 (Biognosys AG, Switzerland). The database is based on the UniProt database (*Hypophthalmichthys nobilis*, version 2023, 431 entries) from uniport, with trypsin selected as the specific enzyme. The fixed modifications were set to carbamidomethyl, while the variable modifications were set to cysteine and methionine oxidation, respectively. The retention time prediction was set to dynamic iRT. Data extraction via Spectronau utilized extensive mass calibration that incorporated iRT calibration and gradient stability to generate an ideal dynamic extraction window.

2.15. Statistical analysis

The statistical analysis of variances, means, and standard errors was carried out using Excel 2017 (Microsoft Office Excel 2017 for Windows). The significant ($P < 0.05$) difference analysis was performed using the SPSS 17.0 program (SPSS 17.0 for Windows, SPSS Inc., Chicago, IL, USA). The One-way ANOVA and Tukey test were utilized to evaluate statistical differences, and graphs were created using Origin 2024 (Origin Lab Co., Northampton, MA, USA).

3. Results and discussion

3.1. Changes in pH and H_2O_2

The changes in pH values and H_2O_2 content of the surimi rinsing wastewater during CAPJ treatment are shown in Fig. 1A. The pH gradually dropped from an initial value of 6.91 to 3.20 ($P < 0.05$) as treatment time increased. The observed decline in the pH was ascribed to the transformation of non-covalently bound reactive plasma

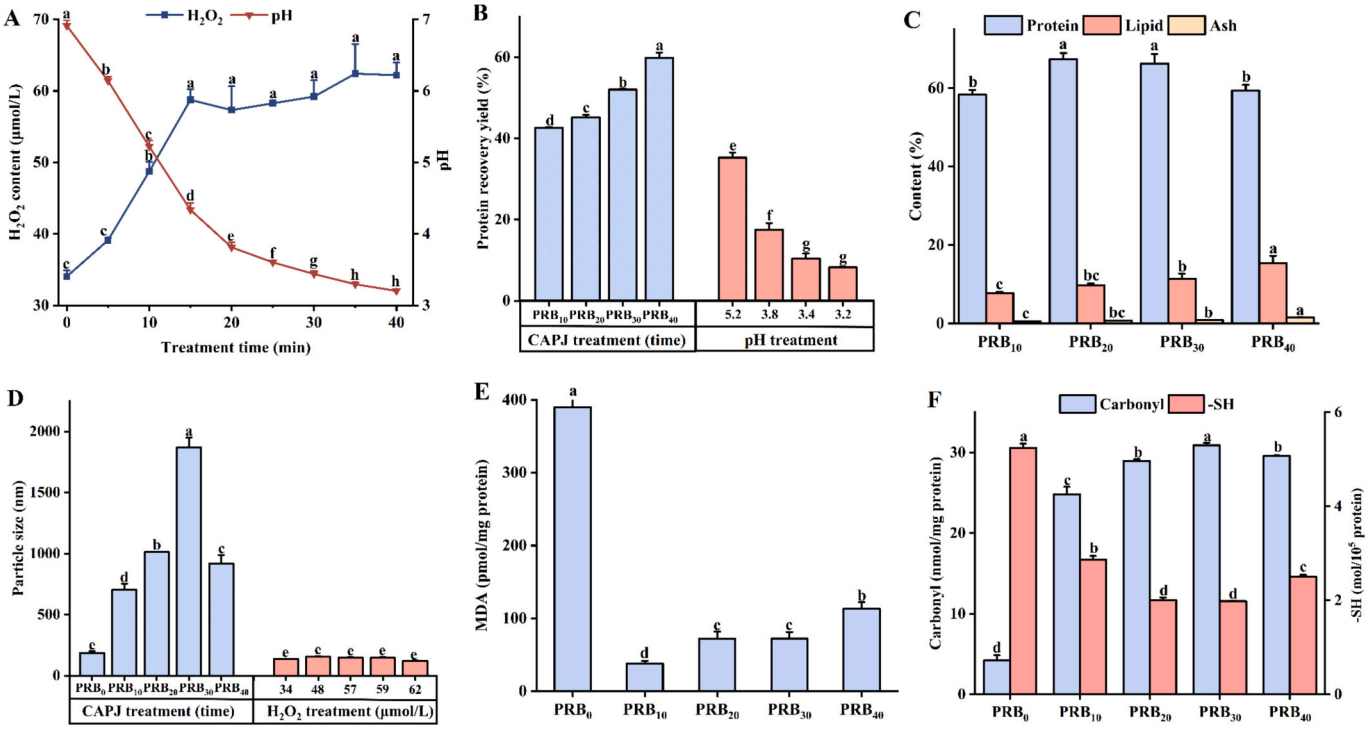

Fig. 1. Changes in pH (A) and H_2O_2 content (A) of surimi rinsing wastewater during CAPJ treatment. Changes in protein recovery yield (B) in CAPJ and pH treatment groups. Changes in basic composition (C) of protein-rich biomass (PRB) from surimi rinsing wastewater treated with CAPJ. Changes in particle size (D) of PRB in CAPJ treatment and H_2O_2 treatment groups. Changes in the content of MDA (E), carbonyl (F), total sulfhydryl group (-SH) (F) of PRB from surimi rinsing wastewater treated with CAPJ. Different lowercase letters indicate significant differences ($P < 0.05$), where lowercase letters indicate the significance of different samples at the same treatment, and capital letters indicate the significance of the same sample at different treatments. The PRB_0, PRB_{10}, PRB_{20}, PRB_{30} and PRB_{40} represent PRB from surimi rinsing wastewater treated with CAPJ at different times (0 min, 10 min, 20 min, 30 min and 40 min), respectively.

components and the exposure of protein fragments or amino acids (Ke et al., 2023). The pH of the protein dispersion dramatically influenced the solubility and conformation of proteins (Tadpitchayangkoon, Park, & Yongsawatdigul, 2010).

Another crucial parameter, the content of H_2O_2 was observed with a significant ($P < 0.05$) increase from 34.05 μmol/L (0 min) to 58.74 μmol/L (15 min) and finally levelled off (Fig. 1A) with the treatment time. The results presented by Li et al. (2022) demonstrated a significant increase in the H_2O_2 content from 8.73 μg/L to 70.82 μg/L over the time extension from 0 s to 240 s. H_2O_2 was the major reactive oxygen species during plasma discharge with strong oxidation to induce protein denaturation and aggregation (Li et al., 2021).

3.2. Changes in protein recovery yield

Fig. 1B illustrates the impact of CAPJ and pH treatment on the recovery yield of protein from the surimi rinsing wastewater. CAPJ treatment (10–40 min) positively affected the protein recovery yield ($P < 0.05$), and the opposite of pH treatment (5.2–3.2). The CAPJ-treated sample exhibited a significant increase in protein recovery yield ($P < 0.05$) compared to the pH-treated sample, with the PRB_{40} showing the highest value (59.84 %). However, the recovery yield of the sample adjusted to 3.2 (pH) was the same as that of PRB_{40} (8.23 %) in Fig. 1B. Therefore, pH was unlikely to be the only factor dictating the higher protein recovery yield exhibited by the CAPJ treatment. These results were consistent with Ekezie et al. (2019), who observed a significant decline in protein solubility after cold plasma treatment.

3.3. Composition of PRB

The values of PRB composition are displayed in Fig. 1C. The protein content in all PRB was >58 %, and PRB_{20} was the highest (67.39 %), implying a protein-dominated system. The crude protein content exhibited an incremental trend with increasing treatment time but decreased at PRB_{40}. The time of CAPJ treatment affected the type and concentration of active substances produced, which in turn changed the surface proteins and protein-related compounds, causing fluctuations in protein content. When the protein was recovered via CAPJ treatment, nonprotein substances such as lipids and ash in the surimi rinsing wastewater might also be extracted and co-precipitated, with consequences for the purity of the final protein product (Zhang et al., 2022). The lipid content of the CAPJ treatment was lower than that reported for other recovery methods, such as isoelectric point precipitation (18.19 %) and pH-shifting (12.59 %), indicating the consideration of CAPJ treatment as an effective method to reduce lipid content in the recovered PRB (Ren et al., 2024). The ash content of recovered PRB was in the range of 0.51 % to 1.51 %, which was lower compared with a study where the reported ash content was in the range of 7.42 % to 8.59 % (Ren et al., 2024). Moreover, the recovery of PRB may potentially contain moisture and polysaccharides (Gehring et al., 2011).

3.4. Changes in particle size of protein aggregates

Protein particle size is a crucial parameter for evaluating the deposition capacity of proteins (Ekezie et al., 2019). Proteins in surimi rinsing wastewater had a smaller particle size due to the presence of natural forms. Overall, the particle sizes of protein aggregates were smaller than that of treated protein by CAPJ (Fig. 1D). Furthermore, the particle sizes of protein aggregates treated by H_2O_2 was markedly smaller than that in the CAPJ treatment group containing the same concentration of H_2O_2. It suggested that the aggregation of proteins was induced not only by the oxidation of H_2O_2. The particle size of subsided proteins with different times of CAPJ treatment changed to bigger, and at PRB_{30}, the size was 1869.08 nm (Fig. 1D). The continuous energetic plasma substances produced by the CAPJ treatment may lead to protein unfolding and enhance protein-protein interaction, ultimately resulting in protein aggregation, which is reflected in the increase in particle size (Luo et al., 2022). However, the particle size of protein in CAPJ treatment exhibited a rapid ($P < 0.05$) decrease with prolonged time (> 30 min), reaching 918.08 nm at PRB_{40} (Fig. 1D). Energetic particles could destroy peptide bonds, including $O_2^{-\bullet}$ and OH• radicals produced during CAPJ treatment by etching, reducing particle size (Liu et al., 2024).

3.5. Changes in lipid oxidation

The TBARS value reflected the degree of lipid oxidation and could be shown by the content of MDA (Li et al., 2023). The surimi rinsing wastewater contained a small number of lipids (Fig. 1C), which could potentially result in the generation of lipid oxidation products (Tadpitchayangkoon et al., 2010). The significant ($P < 0.05$) decrease in TBARS content in the CAPJ-treated group compared to PRB_0 (Fig. 1E), which was attributed to the ability of the reactive substances produced by the CAPJ treatment to react with MDA leading to the reduction (Ke et al., 2023). In contrast, the TBARS content of the recovered PRB samples gradually ($P < 0.05$) increased with CAPJ treatment (10–40 min) (Fig. 1E), suggesting that the lipid was also undergoing oxidation by CAPJ treatment of surimi rinsing wastewater. The results of Liu et al. (2023) for tilapia fillets treated with cold plasma confirmed the plasma treatment's ability to oxidize lipid. Meanwhile, lipid oxidation during CAPJ treatment could facilitate the oxidation of proteins in the surimi rinsing wastewater as well (Li et al., 2023). The TBARS contents of PRB_0, PRB_{10} and PRB_{40} were 390.08, 38.21 and 113.27 pmol MDA/mg protein (Fig. 1E), respectively. These values fell within the range of 10 to 2300 pmol MDA equivalents/mg, which has been reported for fresh dietary lipids (Jiang et al., 2022).

3.6. Modifications of amino acid side chains

3.6.1. Carbonyl and -SH contents

The extent of protein oxidation following CAPJ treatment was investigated through the assessment of carbonyl and -SH content modifications in the recovered PRB (Luo et al., 2022). In general, protein oxidation modified amino acid side chains and protein polypeptide backbones, affecting protein functions including protein solubility and recovery yield (Cheng et al., 2023).

As illustrated in Fig. 1F, the carbonyl content in PRB_{30} (30.92 nmol/mg protein) rose 7.36 ($P < 0.05$) times relative to that of PRB_0 (4.20 nmol/mg protein). In PRB_{40}, a significant ($P < 0.05$) reduction to 29.58 nmol/mg protein was observed (Fig. 1F). The results demonstrated that the carbonyl content of protein was significantly influenced by plasma substance exposure time. The active substances generated by the CAPJ treatment could fragmentate the protein backbone via α-amidation and β-scission in addition to direct or indirect mechanisms, as well as oxidizing amino acid side chains to form carbonyl derivatives (Estevez, 2011; Segat et al., 2015). The carbonyl reduction may be due to the cross-linking between the carbonyl derivatives and the nucleophile (ε-amino acid) in the protein (Guo & Xiong, 2019).

The protein treated with CAPJ showed a progressive reduction in the content of -SH (Fig. 1F). The -SH were 0.55, 0.38, 0.38, and 0.48 times ($P < 0.05$) in PRB_{10}, PRB_{20}, PRB_{30}, and PRB_{40} compared to that of PRB_0 (Fig. 1F), respectively. The reduction in.

-SH indicated that the generated plasma reactive substances caused oxidation of the sulfur-containing protein side chains or formation of disulfide-bonded aggregates through covalent cross-linking (Zhang, Fang, et al., 2018). The reactive -SH had a crucial role in the process of protein folding and stability (Gao et al., 2023). These presented results are correlated with previous investigations on MPs and whey protein (Segat et al., 2015; Sharifian et al., 2019).

3.6.2. Dityrosine and Schiff bases

In the presence of free radicals, dityrosine is formed by binding two monomeric tyrosine radicals, which leads to protein cross-linking and

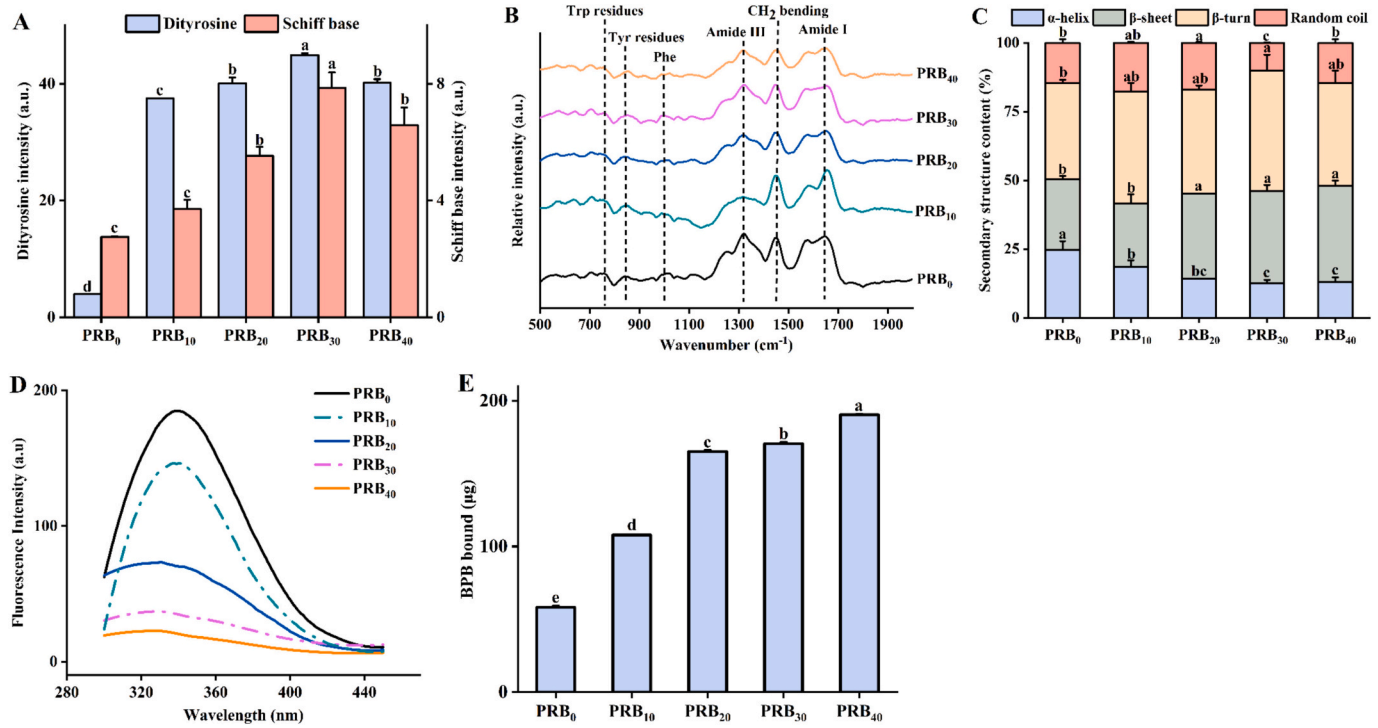

Fig. 2. Changes in dityrosine (A), Schiff base (A), Raman spectrum (B), secondary structure content (C), tertiary structure (D), and surface hydrophobicity (E) of PRB from surimi rinsing wastewater treated with CAPJ. Different lowercase letters indicate a significant difference ($P < 0.05$). The PRB_0, PRB_{10}, PRB_{20}, PRB_{30} and PRB_{40} represent PRB from surimi rinsing wastewater treated with CAPJ at different times (0 min, 10 min, 20 min, 30 min and 40 min), respectively.

aggregation (Zhang, Ma, et al., 2018). With the treatment time, the dityrosine content increased firstly (0–30 min), then down (Fig. 2A), and always higher than PRB_0. As observed in the content of carbonyl groups (Fig. 1F), the highest content of dityrosine was identified in PRB_{30}, which was associated with the higher density of plasma reactive substances at the 30 min treatment time. The reaction between dityrosine and OH· may lead to a decrease after 30 min (Xiong et al., 2009).

Schiff bases were formed via the interaction between the amino acid residues in proteins and the aldehyde from lipid oxidation (Li et al., 2023). The content of Schiff bases was significantly ($P < 0.05$) increased by the CAPJ treatment from 0 to 30 min, then declined in PRB_{40} (Fig. 2A). The result was consistent with the change in carbonyl content (Fig. 1F) and coincided with the findings of Liu et al. (2024). Furthermore, combining the changes in TBARS values (Fig. 1E), we inferred that lipid oxidation may potentially promote protein oxidation.

In summary, CAPJ treatment potentially induced the oxidation of protein amino acid side chains. This oxidation process could foster cross-linking between proteins, decreasing the number of active sites available on the protein surface and reducing solubility.

3.7. Changes in protein structure

3.7.1. Secondary structure

As shown in Fig. 2B, the Raman spectra of the protein revealed the presence of three regions: amide III region (1335–1200 cm^{-1}), amide II region (1600–1500 cm^{-1}) and amide I region (1700–1600 cm^{-1}) (Sharifian et al., 2019). The graphs exhibited comparable patterns after CAPJ treatment, indicating no functional groups were formed or eliminated. A greater peak area was at 1650 cm^{-1} in PRB_0, indicating a higher α-helix content before the CAPJ treatment. The amide III region showed the same decline in intensity (Fig. 2B), revealing a drop in all conformations. Disulfide bonds were frequently represented by the peaks in the 510–540 cm^{-1} range (Zhang et al., 2021). The CAPJ-treated PRB showed an enhanced peak at 540 cm^{-1} (6.96 in PRB_{40}), compared to PRB_0 (3.81). The result was consistent with the change of -SH (Fig. 1F). The increase in disulfide bonds could reflect the formation of protein aggregates and the decrease in protein solubility (Sharifian et al., 2019).

The secondary structures of proteins were determined by the second derivative analysis of the amide I region in Raman spectra. As treatment time increased, the α-helix decreased gradually ($P < 0.05$), opposite to β-turn and β-sheet (Fig. 2C). After 40 min of CAPJ treatment, the α-helix reduced by 11.15 %, whereas the β-sheet and β-turn rose by 9.16 % and 2.73 % ($P < 0.05$), respectively (Fig. 2C). These results demonstrated that CAPJ treatment facilitated the transition from α-helix to β-sheet and β-turn through protein denaturation and unfolding, as well as the modification of amino acid side chain groups (Cheng et al., 2021; Gao et al., 2023). The unwinding and unfolding of α-helix lead to the exposure of functional groups, promoting protein aggregation and interactions (Ekezie et al., 2019).

3.7.2. Tertiary structure

Fluorescence intensity changes can be used as a measure of the extent of protein tertiary structure unfolding (Gao et al., 2023). All plasma-treated PRB showed lower FI_{max} than native PRB_0 and reached a minimum FI_{max} in PRB_{40} (Fig. 2D). The decrease in FI_{max} after CAPJ treatment could be explained by the hydroxylation and nitration of Tryptophan (Trp) and the change in the three-dimensional structure of protein or protein-protein interactions (aggregation) (Cheng et al., 2021). Furthermore, aromatic amino acids were susceptible to attack by reactive substances, resulting in the formation of carbonyl groups through hydroxylation (Fig. 1F). After 40 min of CAPJ treatment, the λ_{max} of Trp was observed to shift from 339.07 nm (PRB_0) to 327.07 nm (PRB_{40}) (Fig. 2D). These results showed that a more compact tertiary protein structure was formed, which prompted the Trp to reside in a more hydrophobic environment (Li et al., 2024).

3.7.3. Surface hydrophobicity

Surface hydrophobicity strongly influenced intermolecular interactions of proteins and revealed the relative number of surface

hydrophobic groups (Ekezie et al., 2019). The rise from 58.15 μg of PRB_0 to the maximum of 190.49 μg in PRB_{40} was observed to be significant ($P < 0.05$) (Fig. 2E). The formation of protein oxidation by-products, such as dityrosine (Fig. 2A), has been observed to enhance the surface hydrophobicity of proteins during plasma treatment (Luo et al., 2022). However, the rise in surface hydrophobicity was ascribed to the exposure of hydrophobic amino acids and a significant increase in denaturation associated with unfolding the structure induced by CAPJ (Fig. 2C) (Cheng et al., 2021). The unfolding of the protein structure and the exposure of hydrophobic groups promoted the aggregation of proteins via chemical interactions/hydrophobic interactions (Liu et al., 2023).

3.8. Changes in isoelectric point (pI)

The pI is critical to protein function and is influenced by the amino acid residues' type, quantity modifications and molecular structures (Yu et al., 2023). When pH approaches the pI, protein tends to gather, and the solution turbidity rises. The precipitate progressively increased with the CAPJ treatment (Fig. 3A). As the pH rose from 3.4 to 6.4, the solution turbidity in all samples rose and subsequently ($P < 0.05$) dropped, and the peak values were at pH 5.8 (PRB_0), 5.2 (PRB_{10}), 4.9 (PRB_{20}), 4.9 (PRB_{30}) and 4.6 (PRB_{40}), respectively (Fig. 3B). The result showed that the CAPJ treatment shifted the pI of protein towards the acidic region. The environment to which the protein was exposed changed due to CAPJ-induced changes in the secondary and tertiary structure of the protein (Fig. 2C, D), which affected the charge balance of protein solution and electrostatic interactions between proteins (Chen et al., 2017; Cheng et al., 2021; Li et al., 2022). The pI change could also affect the net charge (Fig. 3C) and the aggregate behavior of the protein. The formation of spatial site resistance by aggregates in hydrophobic environments may also facilitate protein self-assembly and precipitation (Fig. 2D, E) (Liu et al., 2023).

3.9. SDS-PAGE

The protein profiles of PRB were determined through SDS-PAGE analysis, and the intensity of each band was subsequently analyzed using Image J. As illustrated in Fig. 3D, the predominant profiles of all samples were situated between 30 and 66 kDa, suggesting that they were primarily comprised of SPs. The majority of SPs were made up of enzymes connected to metabolism that produce energy (Tadpitchayangkoon et al., 2010). Nevertheless, the samples exhibited bands within the 175–270 kDa range, indicative of myofibrillar profile (Fig. 3D). The results demonstrated that the protein composition of PRB was intricate, exhibiting the presence of MPs rather than simple SPs. With the increase of CAPJ treatment time, the intensity of bands around 107, 58, 49, 39, 28, and 11 kDa reduced dramatically (Fig. 3D). Except

Table 2
Protein identification results of selected bands in SDS-PAGE.

Band ID	Protein identification	Accession no.	Avg. Mass	Molecular function
Band 1	Ca^{2+}-ATPase	A0A3N0Y1Y9	107,509	Calcium signaling related
Band 2	Pyruvate kinase	A0A1L1YNZ8	58,194	Glycolysis
Band 3	Creatine kinase	A0A3N0XY33	49,193	Energy metabolism
Band 4	Fructose-bisphosphate aldolase	A0A162BDB6	39,678	Glycolysis
Band 5	Tropomyosin alpha-1 chain	A0A3N0XT29	38,682	Muscle structure
Band 6	Phosphoglycerate mutase	A0A3N0YMR5	28,830	Glycolysis
Band 7	Parvalbumin	A0A4Y5R730	11,533	Muscle structure

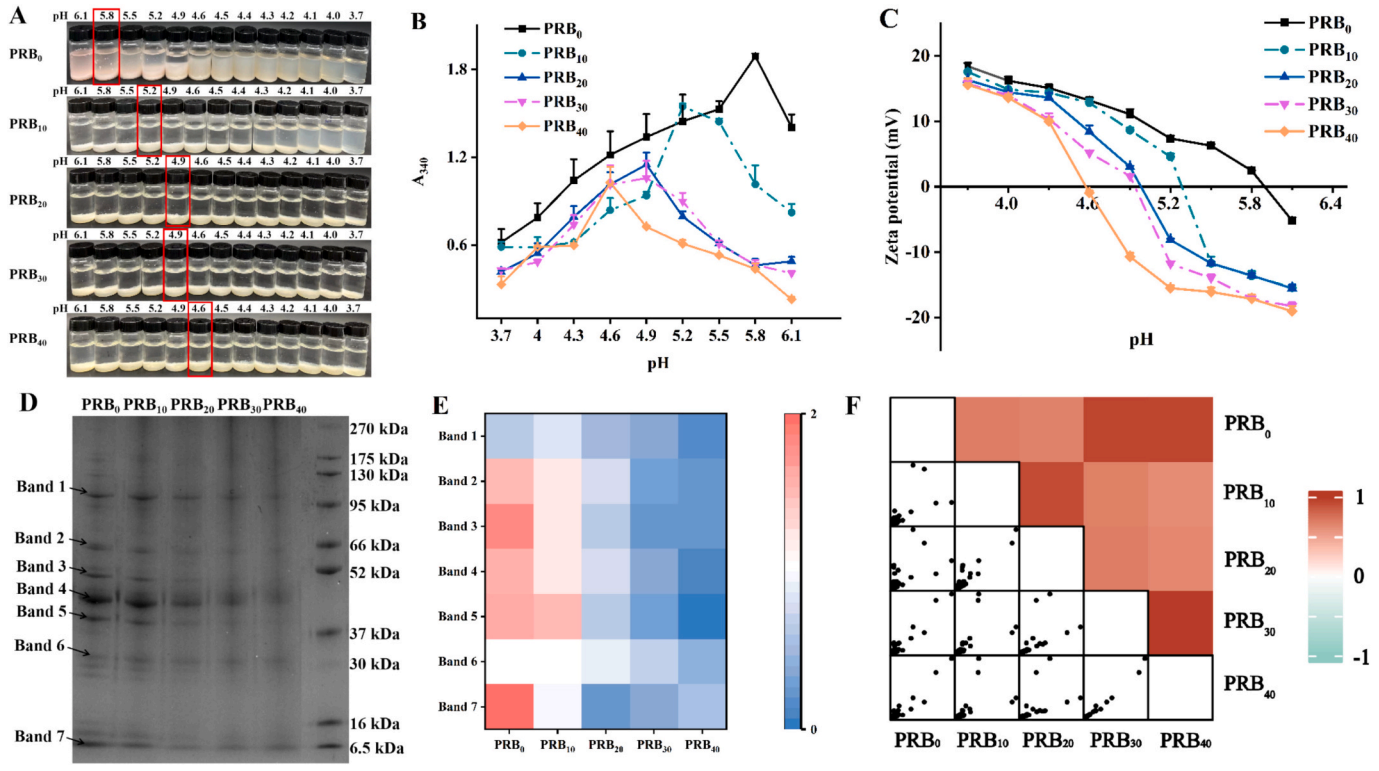

Fig. 3. Changes in the state of the protein glue in different pH (A), turbidity (B), and zeta-potential (C) of PRB solution from surimi rinsing wastewater treated with CAPJ under different pH. SDS-PAGE patterns (D) of PRB and the band intensity (E) of SDS-PAGE. Correlation analysis (F) in PRB_{10} vs PRB_0, PRB_{20} vs PRB_0, PRB_{30} vs PRB_0, and PRB_{40} vs PRB_0. The PRB_0, PRB_{10}, PRB_{20}, PRB_{30} and PRB_{40} represent PRB from surimi rinsing wastewater treated with CAPJ at different times (0 min, 10 min, 20 min, 30 min and 40 min), respectively.

for band 1 and band 7, other band intensities were rated as follows: $PRB_0 > PRB_{10} > PRB_{20} > PRB_{30} > PRB_{40}$ (Fig. 3E). Ca^{2+}-ATPase (Band 1) is an oxidatively sensitive protein (Table 2), and its activity could be significantly affected by ROS produced from the CAPJ treatment (Wang et al., 2024). Probably due to the degradation of cathepsin B, the intensity of creatine kinase (Band 3) decreased with increasing CAPJ treatment time (Ladrat et al., 2003). In addition, as a major constituent of MP tropomyosin (Liu et al., 2024), the tropomyosin α-1 chain (Band 5, around 38 kDa) was degraded (Table 2). From PRB_0 to PRB_{40}, the intensity of the protein polymer gradually increased in the range of 175–270 kDa, indicating that CAPJ treatment induced protein cross-linking. Li et al. (2024) also reported the occurrence of oxidation-induced intermolecular cross-linking and aggregation among proteins.

3.10. DIA proteomics

3.10.1. Composition of recovered PRB

DIA proteomics analysis was utilized to assess the relative content of specific proteins in PRB under different CAPJ treatments. Perform a series of quality controls on the data to ensure the reliability of the results. The precursor level's Qvalue (FDR) cutoff was 1 %, and the protein level was 1 %. A total of 14,079 peptides, 2504 identified protein groups, and 17,646 precursors were detected. The total number of proteins identified from the PRB_0, PRB_{10}, PRB_{20}, PRB_{30} and PRB_{40} was 1894, 2093, 2237, 2095, and 2080, respectively. The correlation values of PRB_{10} with PRB_0 and PRB_{20} with PRB_0 were 0.70 and 0.67 (Fig. 3F), respectively. These results indicated that the proteins recovered by CAPJ treatment contained a substantial number of differentially abundant proteins due to different treatment times.

3.10.2. Identification of differentially expressed proteins (DEPs)

As shown in Fig. 4A, PRB_{10} vs PRB_0 had 549 up-regulated and 664 down-regulated DEPs, PRB_{20} vs PRB_0 had 612 up-regulated and 733 down-regulated DEPs, PRB_{30} vs PRB_0 had 527 up-regulated, and 760 down-regulated DEPs, and PRB_{40} vs PRB_0 had 539 up-regulated and 771 down-regulated DEPs. These results showed that the protein content in the PRB changed significantly during CAPJ treatment. The expression of a substantial number of enzyme proteins was down-regulated, including a variety of amino acid and carbohydrate metabolic enzymes (Table 3). These substances are the main cause of the deterioration of the surimi gel and are the primary components removed from the surimi during rinsing (Xu et al., 2024). As a result of the attack by the active substance,

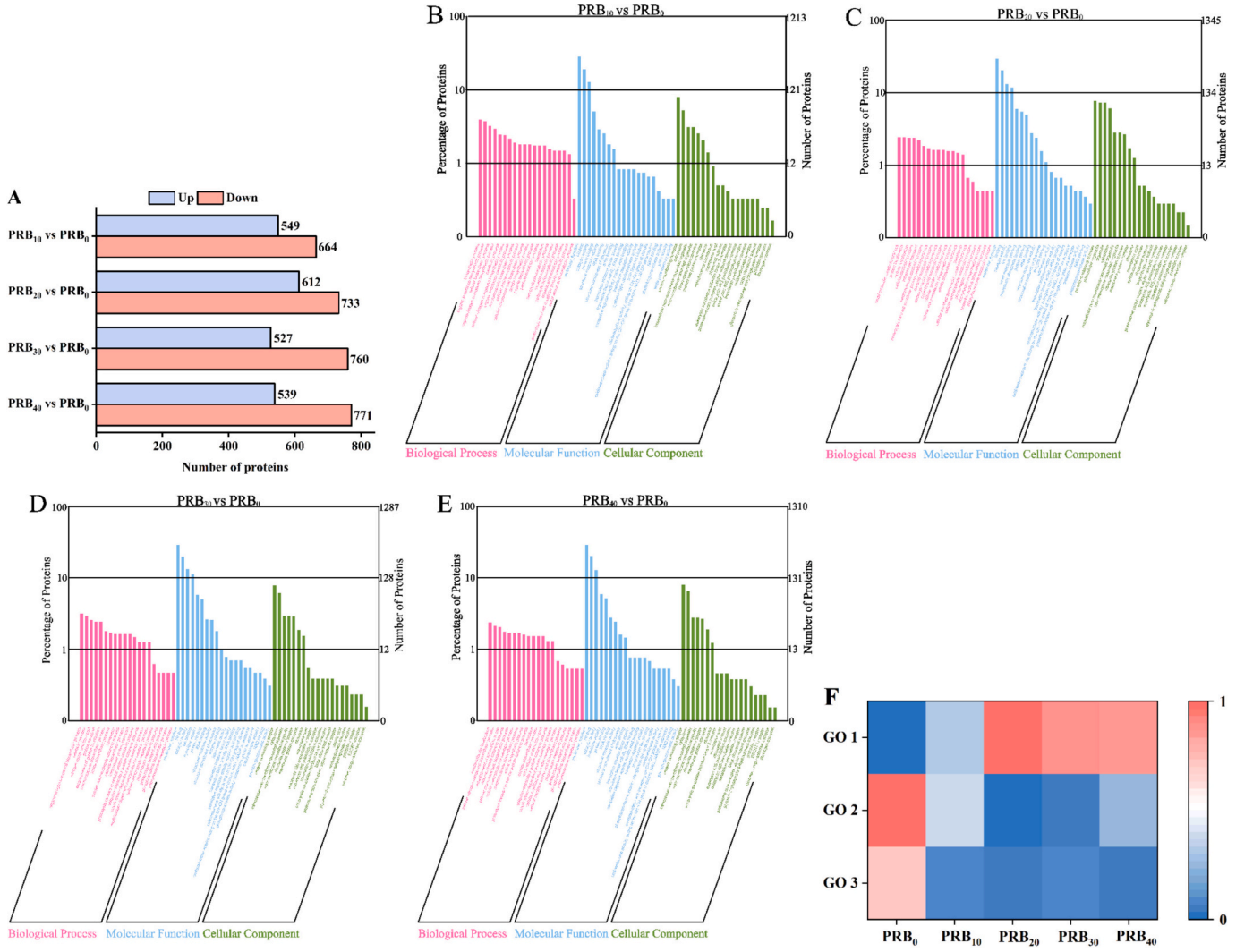

Fig. 4. The number of differentially expressed proteins (DEPs) (A) in PRB_{10} vs PRB_0, PRB_{20} vs PRB_0, PRB_{30} vs PRB_0, and PRB_{40} vs PRB_0. Gene Ontology (GO) classification of DEPs in PRB_{10} vs PRB_0 (B), PRB_{20} vs PRB_0 (C), PRB_{30} vs PRB_0 (D), and PRB_{40} vs PRB_0 (E). The abundance of GO (F) is categorized as GO1, GO2 and GO3 in PRB_0, PRB_{10}, PRB_{20}, PRB_{30} and PRB_{40} DEPs. GO1, GO2 and GO3 represent energy derivation by oxidation of organic compounds (GO:0015980), response to oxidative stress (GO:0006979) and antioxidant activity (GO:0016209) items, respectively. The PRB_0, PRB_{10}, PRB_{20}, PRB_{30} and PRB_{40} represent PRB from surimi rinsing wastewater treated with CAPJ at different times (0 min, 10 min, 20 min, 30 min and 40 min), respectively.

Table 3
Special type of DEPs of in protein-rich biomass (PRB) by CAPJ treatment. PRB_0, PRB_{10}, PRB_{20}, PRB_{30}, and PRB_{40} refer to proteins subjected to 0 min, 10 min, 20 min, 30 min and 40 min CAPJ treatment, respectively.

Accession	Description	Regulate (SP_{10} vs SP_0)	Regulate (SP_{20} vs SP_0)	Regulate (SP_{20} vs SP_0)	Regulate (SP_{40} vs SP_0)	Molecular function
A0A9J8DMF8	Parvalbumin	down	down	down	down	Muscle structure
A0A8C1CBN0	Creatine kinase	down	down	down	down	Energy metabolism
A0A9J7XE98	Phosphopyruvate hydratase	down	down	down	down	Glycogen metabolism
A0A9J8BGI0	Fructose-bisphosphate aldolase	down	down	NC	down	Glycolysis
A0A9J8ALK3	Glyceraldehyde-3-phosphate dehydrogenase	down	down	down	down	Glycolysis
A0A9J8C9A0	Triosephosphate isomerase	down	down	down	down	Glycolysis
A0A9J7Y8M2	L-lactate dehydrogenase	down	down	down	down	Carbohydrate metabolism
A0A9J8AEM4	Apolipoprotein A-Ib	down	down	down	down	lipid metabolism
A0A9J8BNA7	Adenylate kinase 1	down	down	down	down	Energy metabolism
A0A9J8CEV4	Pyruvate kinase	down	down	down	down	Glycolysis
A0A9J7YRF6	Peroxiredoxin 2	down	down	down	down	Stress and defense
A0A9J7XHP7	Glucose-6-phosphate isomerase	down	NC	NC	down	Glycolysis
A0A8C1DPP5	Phosphoglucomutase 1	down	down	down	down	Glycolysis
A0A9J8BRJ7	Hemoglobin, alpha adult 1	down	down	down	down	Blood protein
A0A9J7WZV4	Nucleoside diphosphate kinase	down	down	down	down	Signal transduction
A0A9J7XVI4	Glycerol-3-phosphate dehydrogenase [NAD(+)]	down	down	down	down	Glycolysis
A0A9J8DI04	Fatty acid binding protein 3	down	down	down	down	lipid metabolism
A0A9R1SL95	Phosphatidylethanolamine binding protein 1	down	down	down	down	Signal transduction
A0A8C1CJA3	Integrin, alpha 6b	down	down	down	down	Cellular process
A0A9J7YHW5	Heat shock cognate 70	down	down	down	down	Stress and defense
A0A8C1B2C3	Myosin, heavy chain b	up	up	NC	up	Muscle structure
A0A8C1E0Q6	Myosin, light chain 10	up	up	up	up	Muscle structure
A0A8C1B4Q1	Actinin, alpha 1	up	up	up	up	Muscle structure

The "up" or "down" indicates significant ($P < 0.05$) differences in protein abundance between the two groups. NC represents the proreins were no abundance changes in the two groups.

most of the binding sites of the enzyme protein were destroyed (Zhang et al., 2018), causing the enzyme protein to fail to attach to large protein aggregates and precipitate.

Table 3 presents the top 20 proteins with the highest protein quantification to demonstrate their relative expression levels between groups. Twenty common DEPs (Table 3) were found to be less abundant in the PRB_{10}, PRB_{20}, PRB_{30} and PRB_{40} samples than in the PRB_0 samples, with most of the proteins localized to the sarcoplasmic fraction. Proteins associated with myofibrillar fraction were simultaneously discovered in DEPs, and 3 proteins with higher abundance are shown in Table 3. The results revealed that a small amount of protein from the myofibrillar fraction was deposited into the protein recoveries, consistent with the SDS-PAGE result (Fig. 3D). MPs are susceptible to oxidative degradation by ROS formed during CAPJ treatment (Ni et al., 2024), which further led to down-regulation of the expression of related proteins (tropomyosin beta chain and fibrinogen gamma etc., data were not shown). Meanwhile, the small molecules produced by degradation up-regulate the expression of certain proteins including actin-related proteins and myosin light chains (Table 3).

Among the 23 discovered proteins (Table 3), enzymes involved in glycolysis and glycogen (8), muscle contraction or component structural proteins (4), and proteins involved in energy metabolism and signal transduction (4) were the most abundant. The detected hemoglobin was probably from blood (Huang et al., 2011). The abundance of enzymes such as fructose-bisphosphate aldolase, glyceraldehyde-3-phosphate dehydrogenase, and triosephosphate isomerase decreased with CAPJ treatment. These glycolysis and energy metabolism enzymes may be deposited on myofibrillar fraction and bind to myofilaments (e.g., actin) to form protein complexes (Xing et al., 2020). The rise in α-actin fragments during CAPJ treatment confirmed that the thin filaments were degraded, probably resulting in a soft structure of the thin filaments (Kjærsgård et al., 2006). As a soluble calcium-binding protein, the parvalbumin is susceptible to reactive oxygen substances (Wang et al., 2024).

Gene Ontology (GO) analysis was employed to categorize differentially abundant proteins into three functional groups (biological process, molecular function, and cellular component) (Fig. 4B, C, D, E). The distribution and convergence of DEPs were comparable at various CAPJ treatment times, although there were considerable variances. Almost all biological processes in the functional groups were associated with ROS, signaling mediators of cellular life activities (Liu et al., 2022). The abundance of DEPs categorized as energy derivation by oxidation of organic compounds (GO:0015980), response to oxidative stress (GO:0006979) and antioxidant activity (GO:0016209) items in the biological processes and molecular function annotations was shown in Fig. 4F. As the duration of CAPJ treatment increased, several proteins involved in energy derivation by oxidation of organic compounds, including phosphorylase b kinase regulatory subunit and glycogen synthase, were up-regulated due to external oxidative attack. Glutathione peroxidase (GO:0006979) and peroxiredoxin-6 (GO:0016209), enzymes of cellular defense against oxidative stress, were significantly expressed (Li et al., 2022). These two enzymes could attenuate protein oxidation caused by ROS (Moon et al., 2019). In the study, the expression levels of these two antioxidant enzymes indicated that the proteins activated antioxidant defenses in response to oxidative damage induced by CAPJ treatment.

Based on the results above, we speculated that the activity of these antioxidant enzymes might be decreased by the oxidation modification from the CAPJ treatment, or the increased antioxidant function of enzymes was far from offsetting the oxidation. These resulted in the oxidation of protein and promoted its aggregation and recovery.

4. Conclusion

CAPJ technology was evaluated to recover PRB from surimi rinsing wastewater. A treatment time of 40 min was demonstrated to yield the highest protein recovery. The CAPJ treatment induced the protein structure to unfold and exposed more hydrophobic groups. Oxidation resulted in the loss of -SH and the formation of carbonyl groups while simultaneously promoting larger particle size. Proteomics showed that

the treatment time influenced the composition of the recovered proteins by plasma treatment. It can be hypothesised that protein modifications and structural changes induced by active substances are the driving forces in the recovery of PRB from surimi rinsing wastewater using CAPJ technology. Further investigations are essential to determine the specific and safe recovered protein levels for industrial applications.

CRediT authorship contribution statement

Xin Wang: Writing – review & editing, Writing – original draft, Methodology, Investigation, Formal analysis, Data curation. **Mengzhe Li:** Writing – review & editing, Methodology, Conceptualization. **Tong Shi:** Writing – review & editing, Funding acquisition, Conceptualization. **Abdul Razak Monto:** Writing – review & editing. **Li Yuan:** Writing – review & editing. **Wengan Jin:** Methodology. **Ruichang Gao:** Writing – review & editing, Supervision, Project administration, Funding acquisition, Conceptualization.

Declaration of competing interest

The authors declare that they have no known competing financial interests or personal relationships that could have appeared to influence the work reported in this paper.

Data availability

Data will be made available on request.

Acknowledgments

This project had support from National Natural Science Foundation of China (U20A2067, 32202090), the Agriculture Research System of China of MOF and MARA (CARS-46), the Natural Science Foundation of Jiangsu Province (BK20220520) and the Postdoctoral Research Foundation of China (2022M721389).

References

Chen, X., Tume, R. K., Xu, X. L., & Zhou, G. H. (2017). Solubilization of myofibrillar proteins in water or low ionic strength media: Classical techniques, basic principles, and novel functionalities. *Critical Reviews in Food Science and Nutrition, 57*(15), 3260–3280. https://doi.org/10.1080/10408398.2015.1110111

Cheng, J. H., Chen, Y. Q., & Sun, D. W. (2021). Effects of plasma activated solution on the colour and structure of metmyoglobin and oxymyoglobin. *Food Chemistry, 353*, Article 129433. https://doi.org/10.1016/j.foodchem.2021.129433

Cheng, J. H., Li, J., & Sun, D. W. (2023). Effects of dielectric barrier discharge cold plasma on structure, surface hydrophobicity and allergenic properties of shrimp tropomyosin. *Food Chemistry, 409*, Article 135316. https://doi.org/10.1016/j.foodchem.2022.135316

Ekezie, F. G. C., Cheng, J. H., & Sun, D. W. (2019). Effects of atmospheric pressure plasma jet on the conformation and physicochemical properties of myofibrillar proteins from king prawn (*Litopenaeus vannamei*). *Food Chemistry, 276*, 147–156. https://doi.org/10.1016/j.foodchem.2018.09.113

Estevez, M. (2011). Protein carbonyls in meat systems: A review. *Meat Science, 89*(3), 259–279. https://doi.org/10.1016/j.meatsci.2011.04.025

Gao, S., Liu, Y. Y., Fu, Z. X., Zhang, H. J., Zhang, L. T., Li, B., … Luo, Y. K. (2023). Uncovering quality changes of salted bighead carp fillets during frozen storage: The potential role of time-dependent protein denaturation and oxidation. *Food Chemistry, 414*, Article 135714. https://doi.org/10.1016/j.foodchem.2023.135714

Gehring, C. K., Gigliotti, J. C., Moritz, J. S., Tou, J. C., & Jaczynski, J. (2011). Functional and nutritional characteristics of proteins and lipids recovered by isoelectric processing of fish by-products and low-value fish: A review. *Food Chemistry, 124*(2), 422–431. https://doi.org/10.1016/j.foodchem.2010.06.078

Guo, A. Q., & Xiong, Y. L. (2019). Glucose oxidase promotes gallic acid-myofibrillar protein interaction and thermal gelation. *Food Chemistry, 293*, 529–536. https://doi.org/10.1016/j.foodchem.2019.05.018

Huang, H. G., Larsen, M. R., Karlsson, A. H., Pomponio, L., Costa, L. N., & Lametsch, R. (2011). Gel-based phosphoproteomics analysis of sarcoplasmic proteins in postmortem porcine muscle with pH decline rate and time differences. *Proteomics, 11*(20), 4063–4076. https://doi.org/10.1002/pmic.201100173

Jiang, Y. H., Zhang, C. P., Zhao, X., & Xu, X. L. (2022). Recovery of emulsifying and gelling protein from waste chicken exudate by using a sustainable pH-shifting treatment. *Food Chemistry, 387*, Article 132886. https://doi.org/10.1016/j.foodchem.2022.132886

Ke, Z. G., Bai, Y. W., Yi, Y. Q., Ding, Y. C., Wang, W. J., Liu, S. L., … Ding, Y. (2023). Why plasma-activated water treatment reduced the malonaldehyde content in muscle foods. *Food Chemistry, 403*, Article 134387. https://doi.org/10.1016/j.foodchem.2022.134387

Kjærsgård, I. V. H., Norrelykke, M. R., & Jessen, F. (2006). Changes in cod muscle proteins during frozen storage revealed by proteome analysis and multivariate data analysis. *Proteomics, 6*(5), 1606–1618. https://doi.org/10.1002/pmic.200500252

Ladrat, C., Verrez-Bagnis, V., Noël, J., & Fleurence, J. (2003). In vitro proteolysis of myofibrillar and sarcoplasmic proteins of white muscle of sea bass (*Dicentrarchus labrax* L.): Effects of cathepsins B, D and L. *Food Chemistry, 81*(4), 517–525. https://doi.org/10.1016/s0308-8146(02)00481-8

Li, J. L., Chen, Y. Q., & Cheng, J. H. (2021). Effect of plasma activated water on the color development of ham. *Food Science, 42*(22), 9–15. https://doi.org/10.7506/spkx1002-6630-20201019-172

Li, M. Z., Shi, T., Wang, X., Bao, Y. L., Xiong, Z. Y., Monto, A. R., … Gao, R. C. (2022). Plasma-activated water promoted the aggregation of *Aristichthys nobilis* myofibrillar protein and the effects on gelation properties. *Current Research in Food Science, 5*, 1616–1624. https://doi.org/10.1016/j.crfs.2022.09.003

Li, M. Z., Shi, T., Wang, X., Bao, Y. L., Xiong, Z. Y., Monto, A. R., … Gao, R. C. (2024). Mechanism of plasma-activated water promoting the heat-induced aggregation of myofibrillar protein from silver carp (*Aristichthys Nobilis*). *Innovative Food Science & Emerging Technologies, 91*, Article 103555. https://doi.org/10.1016/j.ifset.2023.103555

Li, Q., Sun, X. Y., Mubango, E., Zheng, Y. Y., Liu, Y. Y., Zhang, Y. H., … Hong, H. (2023). Effects of protein and lipid oxidation on the water holding capacity of different parts of bighead carp: Eye, dorsal, belly and tail muscles. *Food Chemistry, 423*, Article 136238. https://doi.org/10.1016/j.foodchem.2023.136238

Liu, C., Tang, P. P., Liu, X. B., Liu, J. X., Pan, X. H., Aadil, R. M., … Liu, Z. W. (2024). Cold plasma for enhancing covalent conjugation of ovalbumin-gallic acid and its functional properties. *Food Chemistry, 454*, Article 139753. https://doi.org/10.1016/j.foodchem.2024.139753

Liu, C. C., Wan, J. M., Wang, Y. Y., & Chen, G. (2023). Effects of cold plasma treatment conditions on the lipid oxidation kinetics of Tilapia fillets. *Foods, 12*(15), 2845. https://doi.org/10.3390/foods12152845

Liu, Y. Y., Tan, Y. Q., Luo, Y. K., Li, X. M., & Hong, H. (2024). Evidence of myofibrillar protein oxidation and degradation induced by exudates during the thawing process of bighead carp fillets. *Food Chemistry, 434*, Article 137396. https://doi.org/10.1016/j.foodchem.2023.137396

Liu, Y. Y., Zhang, L. T., Gao, S., Zheng, Y. Y., Tan, Y. Q., Luo, Y. K., … Hong, H. (2022). Proteomic analysis of exudates in thawed fillets of bighead carp (*Hypophthalmichthys nobilis*) to understand their role in oxidation of myofibrillar proteins. *Food Research International, 151*, Article 110869. https://doi.org/10.1016/j.foodres.2021.110869

Luo, J., Xu, W. M., Liu, Q., Zou, Y., Wang, D. Y., & Zhang, J. H. (2022). Dielectric barrier discharge cold plasma treatment of pork loin: Effects on muscle physicochemical properties and emulsifying properties of pork myofibrillar protein. *LWT- Food Science and Technology, 162*, Article 113484. https://doi.org/10.1016/j.lwt.2022.113484

Lv, J., Liu, C., Tang, P. P., Liu, J. X., Aadil, R. M., Cheng, J. H., & Liu, Z. W. (2024). Cold plasma-induced covalent binding with epigallo-catechin 3-gallate: A strategy for antigenicity reduction and antioxidant improvement of β-lactoglobulin. *Food Bioscience, 62*, Article 105205. https://doi.org/10.1016/j.fbio.2024.105205

Moon, S. W., Ahn, C. B., Oh, Y., & Je, J. Y. (2019). Lotus (*Nelumbo nucifera*) seed protein isolate exerts anti-inflammatory and antioxidant effects in LPS-stimulated RAW264.7 macrophages via inhibiting NF-κB and MAPK pathways, and upregulating catalase activity. *International Journal of Biological Macromolecules, 134*, 791–797. https://doi.org/10.1016/j.ijbiomac.2019.05.094

Ni, X., Chen, C., Li, R., Liu, Q., Duan, C., Wang, X., & Xu, M. (2024). Effects of ultrasonic treatment on the structure and functional characteristics of myofibrillar proteins from black soldier fly. *International Journal of Biological Macromolecules, 278*, Article 135057. https://doi.org/10.1016/j.ijbiomac.2024.135057

Ren, Z. Y., Long, S. Y., Kang, N. Z., Shi, L. F., Weng, W. Y., & Huang, Q. L. (2024). Structural and functional properties of sarcoplasmic proteins from silver carp surimi wash water recovered by different methods. *Food Science, 45*(7), 225–232. https://doi.org/10.7506/spkx1002-6630-20230728-304

Segat, A., Misra, N. N., Cullen, P. J., & Innocente, N. (2015). Atmospheric pressure cold plasma (ACP) treatment of whey protein isolate model solution. *Innovative Food Science & Emerging Technologies, 29*, 247–254. https://doi.org/10.1016/j.ifset.2015.03.014

Sharifian, A., Soltanizadeh, N., & Abbaszadeh, R. (2019). Effects of dielectric barrier discharge plasma on the physicochemical and functional properties of myofibrillar proteins. *Innovative Food Science & Emerging Technologies, 54*, 1–8. https://doi.org/10.1016/j.ifset.2019.03.006

Tadpitchayangkoon, P., Park, J. W., Mayer, S. G., & Yongsawatdigul, J. (2010). Structural changes and dynamic rheological properties of sarcoplasmic proteins subjected to pH-shift method. *Journal of Agricultural and Food Chemistry, 58*(7), 4241–4249. https://doi.org/10.1021/jf903219u

Tadpitchayangkoon, P., Park, J. W., & Yongsawatdigul, J. (2010). Conformational changes and dynamic rheological properties of fish sarcoplasmic proteins treated at various pHs. *Food Chemistry, 121*(4), 1046–1052. https://doi.org/10.1016/j.foodchem.2010.01.046

Wang, W. X., Bu, Y., Li, W. Z., Zhu, W. H., Li, J. R., & Li, X. P. (2024). Effects of nano freezing-thawing on myofibrillar protein of Atlantic salmon fillets: Protein structure and label-free proteomics. *Food Chemistry, 442*, Article 138369. https://doi.org/10.1016/j.foodchem.2024.138369

Xing, T., Zhao, Z., Zhao, X., Zhuang, S., & Xu, X. L. (2020). Phosphoproteome analysis of sarcoplasmic and myofibrillar proteins in stress-induced dysfunctional broiler

pectoralis major muscle. *Food Chemistry, 319*, Article 126531. https://doi.org/10.1016/j.foodchem.2020.126531

Xiong, Y. L., Park, D., & Zu, T. (2009). Variation in the cross-linking pattern of porcine myofibrillar protein exposed to three oxidative environments. *Journal of Agricultural and Food Chemistry, 57*(1), 153–159. https://doi.org/10.1021/jf8024453

Xu, M., Ni, X., Liu, Q., Chen, C., Deng, X., Wang, X., & Yu, R. (2024). Ultra-high pressure improved gelation and digestive properties of tai Lake whitebait myofibrillar protein. *Food Chemistry: X, 21*, Article 101061. https://doi.org/10.1016/j.fochx.2023.101061

Yu, Q., Shi, T., Xiong, Z. Y., Yuan, L., Hong, H., Gao, R. C., & Bao, Y. L. (2023). Oxidation affects dye binding of myofibrillar proteins via alteration in net charges mediated by a reduction in isoelectric point. *Food Research International, 163*, Article 112204. https://doi.org/10.1016/j.foodres.2022.112204

Zhang, B., Fang, C. D., Hao, G. J., & Zhang, Y. Y. (2018). Effect of kappa-carrageenan oligosaccharides on myofibrillar protein oxidation in peeled shrimp (*Litopenaeus vannamei*) during long-term frozen storage. *Food Chemistry, 245*, 254–261. https://doi.org/10.1016/j.foodchem.2017.10.112

Zhang, H., Ma, J., Shen, J., Lan, Y., Ding, L., Qian, S., & Chu, P. K. (2018). Comparison of the effects induced by plasma generated reactive species and H_2O_2 on lactate dehydrogenase (LDH) enzyme. *IEEE Transactions on Plasma Science, 46*(8), 2742–2752. https://doi.org/10.1109/tps.2018.2834624

Zhang, X. D., Zhang, Y. Q., Ding, H. C., Zhang, W. H., & Dai, Z. Y. (2022). Effect of washing times on the quality characteristics and protein oxidation of silver carp surimi. *Foods, 11*(16), 2397. https://doi.org/10.3390/foods11162397

Zhang, Z. W., Liu, P. P., Deng, X. R., Guo, X., Mao, X. Y., Guo, X. B., & Zhang, J. (2021). Effects of hydroxyl radical oxidation on myofibrillar protein and its susceptibility to μ-calpain proteolysis. *LWT- Food Science and Technology, 137*, Article 110453. https://doi.org/10.1016/j.lwt.2020.110453

Zhao, X., Xing, T., Wang, Y. Y., Xu, X. L., & Zhou, G. H. (2019). Isoelectric solubilization/precipitation processing modified sarcoplasmic protein from pale, soft, exudative-like chicken meat. *Food Chemistry, 287*, 1–10. https://doi.org/10.1016/j.foodchem.2019.02.085